Original Research Paper

Monitoring film coalescence from aqueous polymeric dispersions using atomic force microscopy: Surface topographic and nano-adhesion studies

Ziyi Yang [a,*], Duncan Q.M. Craig [b,**]

[a] School of Pharmaceutical Science, Jiangnan University, 1800 Lihu Road, Wuxi 214122, China
[b] UCL School of Pharmacy, 29-39 Brunswick Square, London WC1N1AX, UK

ARTICLE INFO

ABSTRACT

The aim of the investigation was to develop the use of topographic and nano-adhesion atomic force microscopy (AFM) studies as a means of monitoring the coalescence of latex particles within films produced from a pharmaceutically relevant aqueous dispersion (Eudragit®NE30D). Films were prepared via spin coating and analysed using AFM, initially via tapping mode for topographic assessment followed by force-distance measurements which allowed assessment of site-specific adhesion. The results showed that colloidal particles were clearly observed topographically in freshly prepared samples, with coalescence detected on curing via the disappearance of discernible surface features and a decrease in roughness indices. The effects of temperature and humidity on film curing were also studied, with the former having the most pronounced effect. AFM force measurements showed that the variation in adhesive force reduced with increasing curing time, suggesting a novel method of quantifying the rate of film formation upon curing. It was concluded that the AFM methods outlined in this study may be used as a means of qualitatively and quantitatively monitoring the curing of pharmaceutical films as a function of time and other variables, thereby facilitating rational design of curing protocols.

1. Introduction

Film coating has been widely used within the pharmaceutical industry for purposes including product protection, sustained release, enteric dissolution and taste masking [1–4]. As a result of safety, economic and environmental concerns, pharmaceutical films prepared via aqueous dispersions have become dominant compared to organic solvent-based systems [5–7]. Commercially available aqueous dispersions are typically
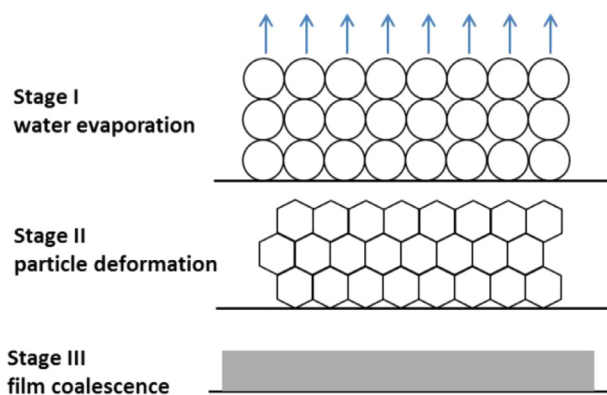
Fig. 1 – Illustration of the three stages of the film formation process prepared using aqueous dispersions.

latex or pseudo-latex systems, comprising colloidal dispersions of polymer in an aqueous base [8]; these are typically applied by a spray coating process to batches of tablets or pellets under continuous agitation at mildly elevated temperatures [9]. A curing process after coating is required to complete coalescence to form a homogeneous and continuous film [10]. It is well established that appropriate curing conditions are necessary to achieve the required performance functionality [6,11], and hence the rational development of curing processes is of considerable interest. Nevertheless, despite the widespread employment of aqueous coating dispersions there remains a need to develop precise quality control methods for film curing, particularly in terms of in situ use. Indeed, identification of the completion of film formation remains reliant on empirical assessment or repetitive dissolution tests [5,12,13].

The mechanism of the film formation process from aqueous dispersions is still under study due to the complexity of the curing process [14,15], although a classic basic model has been suggested which comprises three stages including water evaporation, particle deformation and film coalescence as illustrated in Fig. 1 [8,16]. Water evaporation occurs throughout the entire film formation process, starting from the particle impingement onto the substrate surface during coating to the later stage of film coalescence where water evaporates by diffusing through the formed films in the upper layers [17,18]; consequently, variations in water evaporation rates at different stages of curing having been demonstrated in the literature [19]. More specifically, a constant water evaporation rate close to that of pure water has been suggested when the water content is sufficiently high (solid concentration below 50%, w/w), hence this may be applicable to freshly cast films [20]. Upon curing, more complex mechanisms may be apparent in terms of evaporation route as well as more macroscopic effects such as water evaporation taking place via a drying-front pattern whereby loss occurs principally from the film edge or extremity, creating a transitional dry/wet boundary towards the central wet area which recedes as evaporation continues [21].

Particle deformation also takes place, leading to the formation of void-free structures within the film. The driving forces of the particle deformation process are related to polymer-air, polymer-water and air-water surface interfacial tensions

associated with water evaporation [22–24]. A number of detailed theoretical approaches to explain deformation have been suggested including dry sintering, wet sintering and capillary compaction [22,25,26]. For example, the capillary force resulting from water evaporation from the void between two adjacent particles may be described by considering the particles as elastic bodies, yielding the following relationship:

$$G(t) < 35\gamma_{WA}/R \qquad (1)$$

where $G(t)$ is time-dependent shear modulus, γ_{WA} is water-air surface tension and R is the particle radius [23]. This relationship indicates that the deformation force is inversely proportional to the particle size of the aqueous dispersions [14]. In addition to capillary forces, a compressive force has also been reported to assist the particle deformation whereby the water in the interior of the film must diffuse through the upper layers to evaporate, in turn generating a downwards vacuum-like force to compress the lower particles [27]. Particle deformation is a pre-requisite for coalescence, whereby inter-diffusion of polymers in adjacent particles takes place with the elimination of the intervening boundaries. This polymer inter-diffusion, which is driven by the molecular mobility, enables the formation of a homogeneous and continuous film and has been successfully observed using small angle neutron scattering by monitoring deuterated polymers in the film [28].

From a more empirical and practical viewpoint, the formation of a continuous film is dependent on the minimum film formation temperature (MFFT) which is visually judged by preparing films on a bar with a temperature gradient [29]. The MFFT is generally above the glass transition temperature of the polymers, at which molecular mobility increases allowing inter-diffusion upon curing [30]. However, the interdependence of the three stages mentioned above (evaporation, deformation, coalescence) result in significant difficulties in accomplishing a complete quality control of film curing using conventional microscopic and spectroscopic techniques. In addition, aqueous dispersions in the pharmaceutical industry are multi-component systems which may contain complex mixture of components such as water, polymers, surfactants, co-surfactants, plasticisers and talc; this complexity may further impede development of precise quality control protocols for the film curing process [31].

Overall, therefore, there is a definite need to develop methods by which the film curing process can be assessed and monitored in pharmaceutically relevant film samples, particularly in terms of coalescence as this represents the point at which a continuous and hence functional film is formed. In this study we explored the use of atomic force microscopy (AFM) to monitor the curing process of films composed of a typical pharmaceutical aqueous dispersion, Eudragit®NE30D, prepared using spin coating, as function of curing conditions. Monitoring film curing using AFM has been previously reported [32–34], although the use of AFM as a process development tool for pharmaceutical aqueous latex systems has not been extensively explored. Eudragit®NE30D is composed of a copolymer (ethyl acrylate and methyl methacrylate) and surfactant (Nonoxynol 100) and has been widely applied to the coating of solid dosage forms to sustain drug release. This material is well suited to the development of new quality

control tools due both to its widespread use and pharmaceutical relevance as well as previous reports of changes in drug release profiles from substrates coated by such products on aging [4,13].

Here we use a range of AFM interrogation methods including topography and mechanical adhesion assessment, while we also examine the effects of temperature and humidity on the curing process. Our overall aim is to assess whether AFM may be used as both a quantitative and qualitative method of monitoring the curing process during film formation from aqueous dispersions.

2. Materials and methods

2.1. Materials and sample preparation

Eudragit®NE30D was kindly donated by Evonik Rohm Co.KG, Darmstadt Germany. The product is an aqueous dispersion of a neutral copolymer based on ethyl acrylate and methyl methacrylate with a solid concentration of 30% (w/v). The copolymer has a glass transition temperature of $-8\,°C$ and the minimum film formation temperature of the product is $5\,°C$.

Eudragit®NE30D films were prepared using a G3P-8 spin coater (Specialty Coating System, Surrey, UK). Thin films of Eudragit®NE30D were prepared on microscope cover slides; 0.2 ml of Eudragit®NE30D was dropped onto the cover slide and spun at 2000 rpm for 5 min, resulting in the formation of a transparent thin film. Spin coated films were cured under a range of conditions under ambient humidity unless otherwise specified. More specifically, films were cured at room temperature, $40\,°C$, $60\,°C$, room temperature/0%RH (stored over P_2O_5) and room temperature/100%RH (generated in a sealed chamber with purified water) for different time periods as stated. For films cured at room temperature, $40\,°C$ and $60\,°C$, in order to simulate the actual curing condition in the pharmaceutical industry, the relative humidity was not precisely controlled, and it was only in-door ambient humidity which was measured by a digital humidity monitor every day. During the entire experiment, the humidity for room temperature, $40\,°C$ and $60\,°C$ was measured ranging from 40%RH to 55%RH.

2.2. Atomic force microscopy (AFM) measurements

Atomic force microscopy was performed using a Bruker Multimode 3 (Bruker, Germany) AFM. The cantilever was an antimony doped silicon probe (TESPA, Bruker, Germany) with a spring constant of $42\,Nm^{-1}$ and resonance frequency of 320 kHz. AFM scanning images were achieved in tapping mode. RMS (root-mean-squared) roughness of each AFM height image was calculated using the software of WSxM 5.0 (Nanotec Electronica S.L., Madrid, Spain). In order to minimise sampling effects on the RMS calculation, the largest scanning area ($10 \times 10\,\mu m^2$) provided by the E-scanner was used for the roughness calculation and for each sampling point, 3 AFM scanning images were used to achieve the average RMS roughness.

AFM single point force curve measurements were also performed. The experimental parameters used were as follows: speed of approach and retraction 1.96 µm/s; number of points
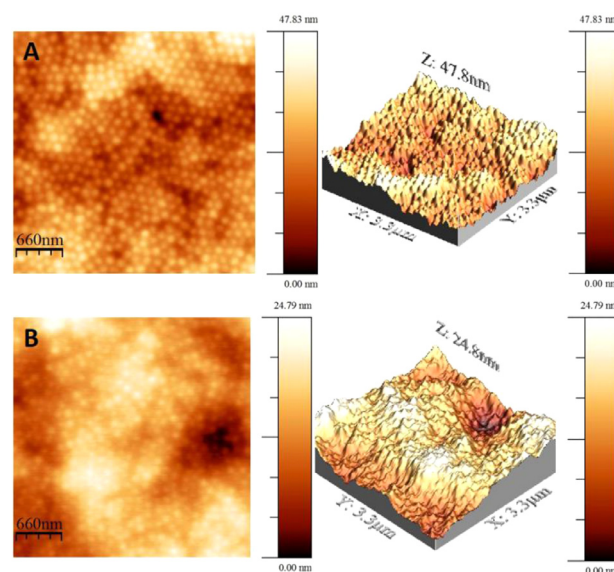

Fig. 2 – AFM height image (2D and 3D on right and left, respectively) of (A) fresh Eudragit®NE30D films and (B) Eudragit®NE30D films cured at 40 °C for 24 h.

512; Z start 0 nm and Z end 1000 nm. These measurements were performed on freshly prepared samples and samples cured for 4, 6, 8, 10, 12, 24 and 48 h at $40\,°C$. For each time point, 10 AFM force curve measurements were conducted.

3. Results and discussion

3.1. Observation of film coalescence on curing using AFM

AFM height images of freshly prepared and cured films (at $40\,°C$ for 24 h) are shown in Fig. 2. In the freshly prepared film (Fig. 2A), colloidal particles with a size of circa 110 nm were observed, which is in agreement with the product information provided by the manufacture in terms of initial dispersion particle size. These particles were configured in close contact, which has been suggested as face centred cubic ordering in the literature [16]. In the 3D version of Fig. 2A, this ordering became more evident, and the morphology of the fresh films resembled the arrangement of particles in the classic model at stage one (Fig. 1).

In order to examine the effects of partial or full coalescence, samples were stored at $40\,°C$, above the MFFT of Eudragit®NE30D ($5\,°C$), for 24 h. Film coalescence was indeed observed after curing under such conditions as shown in Fig. 2B, in which the particle boundaries had become less well defined in comparison to the fresh film but were nevertheless still detectable. This clearly demonstrates the topographic transformation via water evaporation and particle deformation leading to more intimate particle contact and partial coalescence upon curing. However, despite curing well above the MMFT, the film was not yet completely coalesced after 24 h as reflected by the discernible particles in Fig. 2B. It was also observed in the 3D image of Fig. 2B that the peak-to-valley distance (shown as the AFM height image bar) of the film reduced

after curing for 24 h at 40 °C from circa 47 nm to 24 nm. This is in agreement with the suggested film formation process during which the roughness should reduce due to the reduction in particle integrity. More detailed quantification of roughness upon curing will be outlined later.

3.2. Investigation into the effect of curing conditions on film coalescence using AFM

As discussed above, despite curing at 35° higher than the MMFT of Eudragit®NE30D, incomplete film coalescence was observed after 24 h. While we acknowledge that the absence of mechanical agitation and defined air flow may contribute to slower equilibration than expected, it is nevertheless valuable to explore the effects of temperature and storage humidity further using the current model system. Therefore, in this section, the relative importance of curing temperature and humidity to the film coalescence process was evaluated using AFM.

3.2.1. Influence of temperature

The images of films cured at room temperature (48 h), 40 °C (48 h) and 60 °C (24 and 48 h) are shown in Fig. 3. It was observed that after 48 h curing at room temperature, colloidal particles were still evident, and the morphology of this film was nearly identical to the freshly prepared samples (Fig. 2A). In comparison to films cured at room temperature, films cured at 40 °C (Fig. 3B) for 48 h showed a marked reduction in evidence for the presence of colloidal particles, indicating that intact films may have formed. In addition, comparing films cured at 40 °C (Fig. 2B, cured for 24 h) with films cured for 24 and 48 h at 60 °C (Fig. 3C and D) for the same time period, it was seen that the extent of particle coalescence was greater in the film cured at 60 °C than in the film cured at 40 °C. These (initially qualitative) results demonstrate that given the same curing period of time, the curing efficiency is intimately associated with the curing temperature.

The effect of curing temperature on the film coalescence was also reflected by the decreased peak-to-valley roughness from circa 47 nm (Fig. 2A, room temperature for 24 h) to 14 nm (Fig. 4C, 60 °C for 24 h). There are typically three types of roughness measured by AFM: peak-to-valley roughness (the distance between the highest point and the lowest point in the image), mean roughness (the mean value of the surface relative to the centre plane) and RMS roughness (root-mean-squared roughness). RMS roughness has been suggested as the measurement of choice for curing and is defined by [35]:

$$R_{rms} = \sqrt{\frac{\sum_{n=1}^{N} z_n - \bar{z}}{N-1}} \qquad (2)$$

where R_{rms} is the RMS roughness, $\bar{z}$ is the average of the z values (height of each point in the AFM image) within the given areas, z_n is the current z value and N is the number of the data points within the given area. Note that several thousand data points are obtained in this way for each field studied (i.e., each AFM scanning image).

The RMS roughness of films cured under different conditions are summarised in Table 1. Results showed that the RMS roughness reduced from circa 11 nm in fresh films to circa
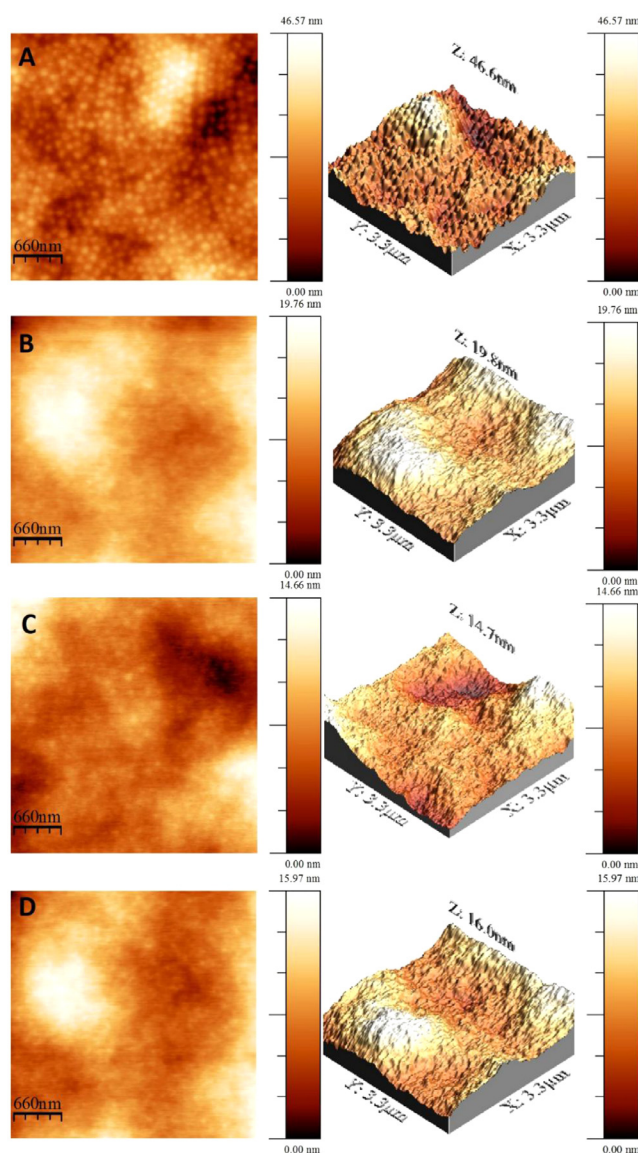

Fig. 3 – AFM height images (left) and 3D version of the height images (right) of (A) Eudragit®NE30D film cured at room temperature for 48 h; (B) Eudragit®NE30D film cured at 40 °C for 48 h; (C) Eudragit®NE30D film cured at 60 °C for 24 h and (D) Eudragit®NE30D film cured at 60 °C for 48 h.

5 nm in coalesced films. Roughness reduction upon curing was further considered in terms of curing rate by monitoring the RMS roughness of films cured at 40 °C for up to 48 h. As seen in Fig. 4, decreased RMS roughness was observed with increasing curing time. An empirical relationship between curing time and RMS roughness was obtained:

$$lnR_{rms} = -0.24 ln t + 2.56 \qquad (R^2 = 0.972) \qquad (3)$$

where R_{rms} is the RMS roughness and t is the curing time.

3.2.2. Influence of humidity

In order to evaluate the effect of humidity on the film formation process, films were cured at room temperature/0%RH and

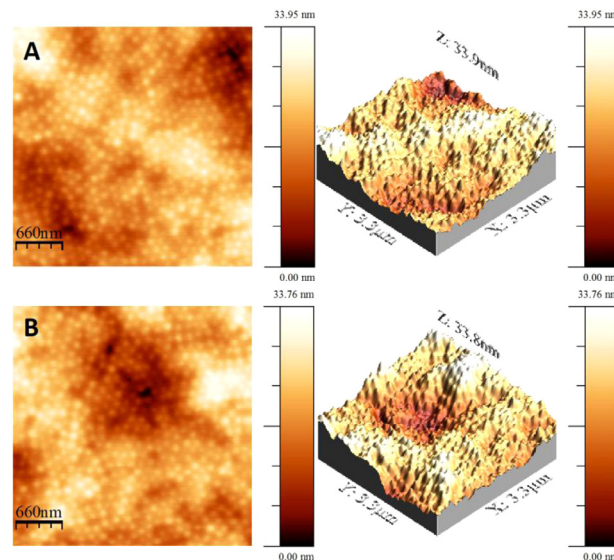| Table 1 – RMS roughness of films cured under different conditions for different periods of time up to 1 month.								
Sample	Fresh	Room temp/48 h	40 °C/24 h	40 °C/48 h	60 °C/24 h	60 °C/48 h	0%RH 25 °C/1 m	100%RH 25 °C/1 m
RMS (nm)	11.2 ± 0.52	9.4 ± 0.47	6.3 ± 0.29	5.1 ± 0.22	4.9 ± 0.25	4.7 ± 0.21	7.2 ± 0.34	7.5 ± 0.41
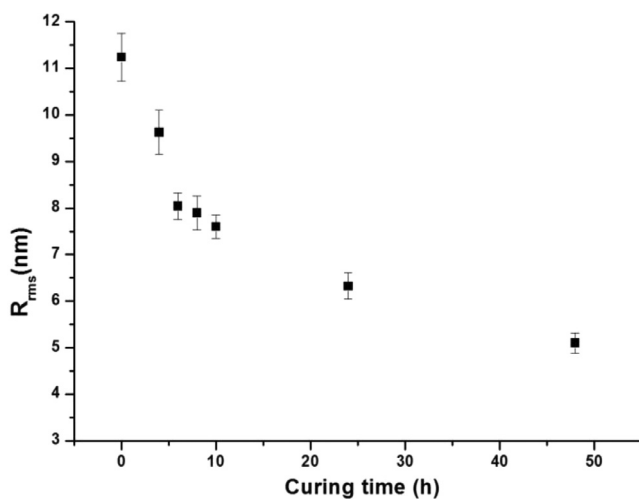
Fig. 4 – RMS roughness of Eudragit®NE30D films cured at 40 °C for up to 48 h (RMS roughness was measured over a scanning area of 10 x 10 µm².

Fig. 5 – AFM height images (left) and the 3D version of height images (right) of (A) Eudragit®NE30D film cured at room temperature/0%RH for 1 month and (B) Eudragit® NE30D film cured at room temperature/100%RH for 1 month.

room temperature/100%RH, respectively, for up to 1 month. It should be noted that room temperature is circa 20 °C higher than the MFFT of Eudragit®NE30D hence, given the time period involved, extensive film coalescence may be expected. It was observed, however, that after 1 month curing under room temperature/0%RH, colloidal particles can still be clearly detected as shown in Fig. 5A. Compared to freshly prepared sample (Fig. 2A), the boundaries of the particles were slightly less well defined after curing under these conditions. Colloidal particles were also detected in samples cured under room temperature/100%RH for 1 month as seen in Fig. 5B. No significant difference in terms of the level of film coalescence was observed when comparing the two samples cured under dry and humid conditions. In addition, the RMS roughness values of the two samples cured under the two different conditions were close (Table 1) and, while smaller than that of the fresh film, were nevertheless markedly higher than the films coalesced at higher temperatures, indicating a dominance of temperature over humidity in determining the rate of curing.

3.3. Evaluation of adhesive and mechanical properties of films

In this study, AFM has been shown to be capable of visualising and quantitatively assessing the topography change of films under different curing conditions. In this section, a further quantitative method based on AFM force curve measurements was employed to measure the mechanical property change of films and the homogeneity of film formation on curing.

AFM force measurements can quantify the adhesion of the surface of the sample to the probe and involve applying the AFM tip onto a substrate and recording the deflection of the cantilever on withdrawal [36]. An annotated example of an AFM force curve measurement conducted on a freshly prepared Eudragit®NE30D film is shown in Fig. 6 in steps. The AFM tip approaches the surface of the film (step A) and, at a very close distance from the surface, the tip is "snapped on" to the surface (step B) as shown in Fig. 6 (enlarged figure) due to the attractive forces between the probe and the sample. Subsequently, the tip is pushed with increasing force against and into the surface (step C). A specified deflection of the probe (to ensure reproducibility of applied force) is used as a trigger point to begin the retraction process (step D). Upon commencing retraction, the adhesive forces provided by the film surface cause the tip to follow a distinct deflection profile (detected and shown as voltage in Fig. 6) compared to that of the tip approach; more specifically, the tip will adhere to the surface, delaying detachment and causing downward deflection (step E) with the corresponding force measured via the maximum deflection voltage compared to the non-contact value (step E), followed by detachment (step F).

In order to quantitatively study the pull-off force, a conversion from the voltage to the actual force with the unit of N was conducted using the spring constant value (42 N/m) of the cantilever provided by the manufacturer. The force conver-
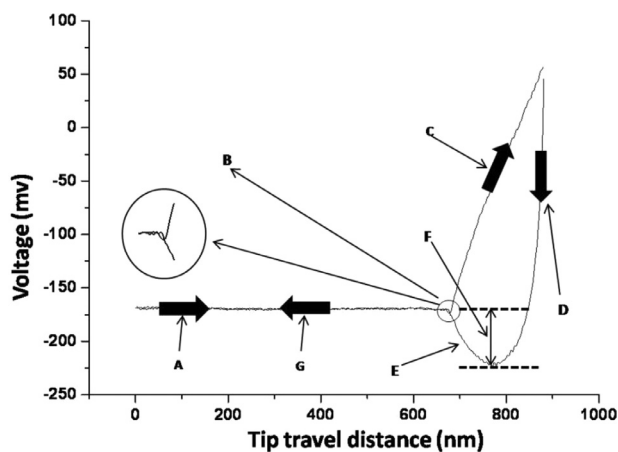
Fig. 6 – AFM force curve measurement of freshly prepared Eudragit®NE30D in steps: (A) the AFM probe approaches from close to the sample surface; (B) "snap on" of the probe on the sample surface due to the attraction force; (C) the AFM probe is further pushed into the surface of the sample; (D) the AFM probe is withdrawn from the sample while still in contact with the surface; (E) the adhesive force from the sample causes the downward deflection of the probe; (F) the AFM pull-off force is registered via the voltage difference between non-contact and the maximum downwards deflection; (G) the AFM probe is removed from the surface.

sion study was carried out by applying a force measurement to a sample with high stiffness, such as glass or mica, in which there was no surface indentation during the entire force curve measurement. The slope of this measurement thus provided the relationship for the distance (nm) deflected by the probe in terms of the voltage signal (V) read by the AFM. The relationship of the conversion study can be described by:

$$\text{conversion rate (nN/V)} = \frac{\text{spring constant of the probe(nN/nm)}}{\text{slope of the measurement(V/nm)}} \tag{4}$$

The actual AFM pull-off force (with the unit of nN) is then obtained by converting the detected deflection value (in Voltage) via Eq. 4. In this study, the conversion study was conducted on a standard AFM calibration grating (TGQ1, NT-MDT, Ireland) which is composed of silicon dioxide. Repeat measurements showed identical slopes which allowed a calibration factor of 1 nm equal to 0.0216 V of cantilever deflection.

AFM pull-off force measurements on films cured at 40 °C for time periods up to 48 h were conducted and the results are shown in Fig. 7. The measured pull-off forces decreased from 87.30 ± 21.25 nN to 18.43 ± 2.28 nN with increasing curing time, indicating a reduced adhesive force with time. The high adhesive force observed for freshly prepared films is compatible with the intended use of aqueous dispersions for coating whereby a high adhesive force enable fresh films to adhere to the solid substrates [31]. It was also noted that the standard deviation of measured pull-off forces decreased with increasing curing time, which may be associated with topographic effects; this is discussed later in the study.
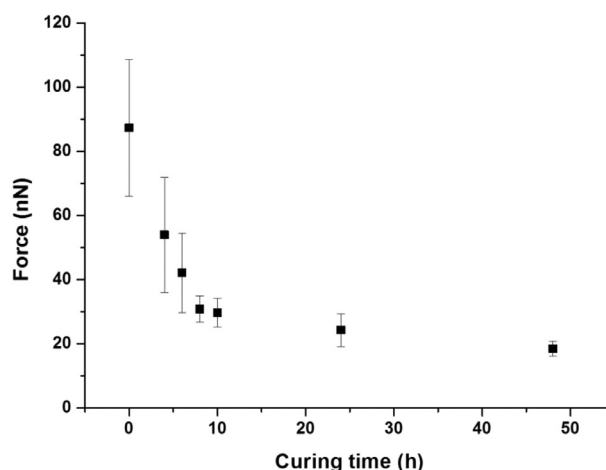

Fig. 7 – AFM pull-off forces measured in films cured at 40 °C for 48 h (for each tested point, $n = 10$).

Pull-off forces of samples cured under a range of conditions are listed in Table 2. It may be seen that for extensively coalesced films, for example films cured at 40 °C and 60 °C for 48 h, the pull-off forces were close to circa 17 nN and were significantly lower than those of the fresh or partially coalesced films. Similarly, films cured at 0%RH and 100%RH at room temperature showed lower pull-off forces for the former (circa 27.74 ± 9.06 nN) than the latter (circa 44.29 ± 11.33 nN), reflecting the greater adhesion of the more hydrated film.

3.4. Investigation into the pull-off force changes on film curing

In this study, AFM was employed to monitor film coalescence from aqueous polymeric dispersions on curing. The study demonstrated that AFM can not only visualise the classic film curing process in terms of progressive disappearance of colloidal particles on curing but it can also quantitatively assess film coalescence by monitoring the topographic (via roughness) and nanomechanical (via adhesion force) changes on curing.

The question naturally arises as to what determines the pull-off force changes on curing. One possibility is the diminishing presence of residual water, although the decreasing variation in the response as the roughness diminishes suggests a strong topographic component to the measurement. It has been reported that the AFM pull-off force (adhesive force) can be affected by geometrical effects with respect to the AFM tip and the tested sample surface as described in the following equation:

$$F_{ad} = \frac{A}{6h_0}\left[\frac{rR}{r+R} + \frac{R}{(1+r/h_0)^2}\right] \tag{5}$$

where F_{ad} is the adhesive force (pull-off force), A is the Hamaker Constant associated with the materials used, h_0 is the distance of the closest approach between the two surface (equal to 0.3 nm as reported in the literature), R is the radius

Table 2 – AFM pull-off force of Eudragit®NE30D films cured under different conditions for different periods of time.

Sample	Fresh	60 °C/2 d	40 °C/2 d	0%RH/1 m [a]	100%RH/1 m [b]
Force (10^{-9} N)	88.78 ± 21.24	16.99 ± 1.84	18.29 ± 2.29	27.74 ± 9.06	44.29 ± 11.33

[a] Eudragit®NE30D film cured under room temperature/0%RH for 1 month.
[b] Eudragit®NE30D film cured under room temperature/100%RH for 1 month.

of the tip of the probe used (8 nm according to the probe manufacture), and r is the radius of the surface asperity [37,38]. In the present case, the only variable in Eq. 5 was the surface asperity radius (r) which is associated with the surface roughness. Therefore, for films at an early stage of curing with high surface roughness, a variety of r values would be expected at the same time point, hence causing the high standard deviation values of the pull-off forces. With progressive film coalescence on curing, the increased flatness of sample surface resulted in more reproducible r values, leading to more reproducible pull-off forces with significantly reduced standard deviations in comparison to fresh films.

The topographic effects on the adhesive pull-off force were further explored using a modification of Eq. 5 in which the influence of RMS roughness is taken into account:

$$F_{ad} = \frac{AR}{6h_0^2}\left[\frac{1}{1 + R/(1.48 \times RMS)} + \frac{1}{(1 + 1.48 \times RMS/h_0)^2}\right] \quad (6)$$

where RMS is the RMS roughness as mentioned above and other parameters have the same meanings as in Eq. 5 [37,38]. The Hamaker Constant is defined by:

$$A = \pi^2 \times C \times \rho_1 \times \rho_2 \quad (7)$$

where ρ_1 and ρ_2 are the number of atoms per unit volume in the two bodies in contact and C is the coefficient in the atom–atom pair potential [39]. As the materials (the AFM probe and the film) in contact during the entire experiment did not change, it can be deduced from the definition that Hamaker Constant in this case study can be assumed to be constant throughout the entire experiment. Therefore, Eq. 6 became a specific relationship describing the effect of surface roughness of the film on the adhesive force measured by AFM (pull-off force) upon curing. This expression indicates that if the surface roughness reduces upon curing, the pull-off force should decrease as well. This is the case for this study, as demonstrated by the respectively measured RMS roughness (Fig. 4) and pull-off force (Fig. 7) values on curing at 40 °C for 48 h, a descending order being observed for both RMS roughness and pull-off force with increasing curing time. This suggests that the observed change in tip adhesion with curing time may have a topographic component as well as being a reflection of the mechanical and adhesive properties of the films.

4. Conclusions

The study has examined the use of AFM to identify and quantify changes in the extent of coalescence of aqueous Eudragit®NE30D films, selected as a model for pharmaceutically relevant latex systems, as a function of time, temperature and humidity. Such information is of considerable importance in determining both the optimal conditions for curing and for ensuring that coalescence has occurred sufficiently to optimise product performance. More specifically, we have demonstrated that the topography of the films may be qualitatively and quantitatively measured (the latter via surface roughness), with coalescence under the conditions studied clearly taking place over protracted time periods, even at elevated temperatures. Care is required with regard to extrapolation of such data to practical situations due to the additional considerations of mechanical agitation and enhanced air flow in a typical film coating process. However as the methods developed here may be easily adapted to 'real' substrate situations then the concept of using these approaches remains relevant and valid. In addition to topography, pull-off force measurements have been utilised as a further quantitative approach, with both the absolute value and the standard deviation being suggested as useful markers for the extent of coalescence.

Declaration of interest

The authors report no conflict of interest.

Supplementary materials

Supplementary material associated with this article can be found, in the online version, at doi:10.1016/j.ajps.2018.09.008.

REFERENCES

[1] Cerea M, Zheng W, Young CR, McGinity JW. A novel powder coating process for attaining taste masking and moisture protective films applied to tablets. Int J Pharm 2004;279(1–2):127–39.

[2] Joshi S, Petereit HU. Film coatings for taste masking and moisture protection. Int J Pharm 2013;457(2):395–406.

[3] Qiao M, Zhang L, Ma Y, Zhu J, Xiao W. A novel electrostatic dry coating process for enteric coating of tablets with eudragit® l100-55. Eur J Pharm Biopharm 2013;83(2):293–300.

[4] Yang ZY, Lu Y, Tang X. Pseudoephedrine hydrochloride sustained-release pellets prepared by a combination of hot-melt subcoating and polymer coating. Drug Dev Ind Pharm 2008;34(12):1323–30.

[5] Yang QW, Flament MP, Siepmann F, Busignies V, Leclerc B, Herry C, et al. Curing of aqueous polymeric film coatings: importance of the coating level and type of plasticizer. Eur J Pharm Biopharm 2010;74(2):362–70.

[6] Felton LA, Porter SC. An update on pharmaceutical film coating for drug delivery. Expert Opin Drug Deliv 2013;10(4):421–35.

[7] Lecomte F, Siepmann J, Walther M, MacRae R, Bodmeier R. Polymer blends used for the coating of multiparticulates: comparison of aqueous and organic coating techniques. Pharm Res 2004;21(5):882–90.

[8] Keddie JL. Film formation of latex. Mater Sci Eng R 1997;21(3):101–70.

[9] Felton LA. Mechanisms of polymeric film formation. Int J Pharm 2013;457(2):423–7.

[10] Kaunisto E, Marucci M, Borgquist P, Axelsson A. Mechanistic modelling of drug release from polymer-coated and swelling and dissolving polymer matrix systems. Int J Pharm 2011;418(1):54–77.

[11] Korasa K, Hudovornik G, Vrečer F. Applicability of near-infrared spectroscopy in the monitoring of film coating and curing process of the prolonged release coated pellets. Eur J Pharm Sci 2016;93:484–92.

[12] Siepmann J, Siepmann F. Stability of aqueous polymeric controlled release film coatings. Int J Pharm 2013;457(2):437–45.

[13] Lin AY, Muhammad NA, Pope D, Augsburger LL. A study of the effects of curing and storage conditions on controlled release diphenhydramine HCL pellets coated with Eudragit® NE30D. Pharm Dev Technol 2003;8(3):277–87.

[14] Steward PA, Hearn J, Wilkinson MC. An overview of polymer latex film formation and properties. Adv Colloid Interface Sci 2000;86(3):195–267.

[15] Irfan M, Ahmed AR, Kolter K, Bodmeier R, Dashevskiy A. Curing mechanism of flexible aqueous polymeric coatings. Eur J Pharm Biopharm 2017;115:186–96.

[16] Winnik MA. Latex film formation. Curr Opin Colloid Interface Sci 1997;2(2):192–9.

[17] Vanderhoff JW, Bradford EB, Carrington WK. The transport of water through latex films. J Polym Sci Polym Symp 2010;41(1):155–74.

[18] Croll SG. Drying of latex paint. J Coat Technol 1986;58(734):41–9.

[19] Sheehan JG, Takamura K, Davis HT, Scriven LE. Microstructure development in particulate coatings examined with cryogenic scanning electron microscopy. Tappi J 1993;76(12):93–101.

[20] Croll SG. Heat and mass transfer in latex paints during drying. J Coat Technol 1987;59(751):81–92.

[21] Denkov ND, Velev OD, Kralchevsky PA, Ivanov IB, Yoshimura H, Nagayama K. Mechanism of formation of two-dimensional crystals from latex particles on substrates. Langmuir 1992;8(12):3183–90.

[22] Kendall K, Padget JC. Latex coalescence. Int J Adhes Adhes 1982;2(3):149–54.

[23] Brown GL. Formation of films from polymer dispersions. J Polym Sci 1956;22(102):423–34.

[24] Dobler F, Pith T, Lambla M, Holl Y. Coalescence mechanisms of polymer colloids: II. Coalescence with evaporation of water. J Colloid Interface Sci 1992;152(1):12–21.

[25] Dillon RE, Matheson LA, Bradford EB. Sintering of synthetic latex particles. J Colloid Sci 1951;6(2):108–17.

[26] Vanderhoff JW, Tarkowski HL, Jenkins MC, Bradford EB. Theoretical consideration of interfacial forces involved in coalescence of latex particles. Rubber Chem Technol 1967;40(4):1246–69.

[27] Sheetz DP. Formation of films by drying of latex. J Appl Polym Sci 1965;9(11):3759–73.

[28] Hahn K, Ley G, Schuller H, Oberthür R. On particle coalescence in latex films. Colloid Polymer Sci 1986;264(12):1092–6.

[29] ASTM. Standard test method for minimum film formation temperature of emulsion vehicles. Philadelphia: ASTM; 1993. p. 104–5.

[30] Winnik MA, Feng J. Latex blends: an approach to zero voc coatings. J Coat Technol 1996;68(852):39–50.

[31] Felton LA, Austin-Forbes T, Moore TA. Influence of surfactants in aqueous-based polymeric dispersions on the thermomechanical and adhesive properties of acrylic films. Drug Dev Ind Pharm 2000;26(2):205–10.

[32] Lin F, Meier DJ. A study of latex film formation by atomic force microscopy. 1. A comparison of wet and dry conditions. Langmuir 1995;11(7):2726–33.

[33] Goudy A, Gee ML, Biggs S, Underwood S. Atomic force microscopy study of polystyrene latex film morphology: effects of aging and annealing. Langmuir 1995;11(11):4454–9.

[34] Xing Y, Xu M, Gui X, Cao Y, Babel B, Rudolph M, et al. The application of atomic force microscopy in mineral flotation. Adv Colloid Interface Sci 2018;256:373–92.

[35] Boussu K, van der Bruggen B, Volodin A, Snauwaert J, van Haesendonck C, vandecasteele C. Roughness and hydrophobicity studies of nanofiltration membranes using different modes of AFM. J Colloid Interface Sci 2005;286(2):632–8.

[36] Cappella B, Dietler G. Force-distance curves by atomic force microscopy. Surf Sci Rep 1999;34(1–3):1–104.

[37] Rabinovich YI, Adler JJ, Ata A, Singh RK, Moudgil BM. Adhesion between nanoscale rough surfaces. I. Role of asperity geometry. J Colloid Interface Sci 2000;232(1):10–16.

[38] Rabinovich YI, Adler JJ, Ata A, Singh RK, Moudgil BM. Adhesion between nanoscale rough surfaces: II. Measurement and comparison with theory. J Colloid Interface Sci 2000;232(1):17–24.

[39] Lee SW, Sigmund WM. AFM study of repulsive van der waals forces between Teflon AF^{TM} thin film and silica or alumina. Colloids Surf A Physicochem Eng Asp 2002;204(1–3):43–50.